Chinese Physics Letters

LETTER

Interference-Controlled Nonclassical Photon Emission via Cavity-Mediated Spin Exchange

Cite as: Jing Tang *et al*. 2026 *Chin. Phys. Lett.* **43** 120402

DOI CSTR

Recommended Articles

Generating Entangled Pairs of Vortex Photons via Induced Emission
D. V. Grosman, G. K. Sizykh, E. O. Lazarev, G. V. Voloshin, and D. V. Karlovets
Chin. Phys. Lett. **42**, 120404 (2025)

Heterogeneous Single-Photon Transistor with Rydberg Atoms
Jian-Hao Yu, Ren Liao, Gen-Sheng Ye, Ze-Rui Song, Jing-Lv Yang, Kuan Zhang, and Lin Li
Chin. Phys. Lett. , (2026)

Twist-Enhanced Thermoelectric Effect in $Cr(pyz)_4$-Based Heterojunction via Tuning Spin Quantum Interference
Li-Hua Luo, Shi-Hua Tan, Xiao-Fang Peng, and Meng-Qiu Long
Chin. Phys. Lett. **43**, 050803 (2026)

Quantum Interference and Optical Tuning of Self-Trapped Exciton State in Double Halide Perovskite
Kai-Xuan Xu *et al*.
Chin. Phys. Lett. **43**, 030703 (2026)

Ultra-Compact Transverse Mode Quantum Interference Device on Silicon
Yang Li *et al*.
Chin. Phys. Lett. **42**, 110603 (2025)

Broadband Telecom Single-Photon Emissions from InAs/InP Quantum Dots Grown by MOVPE Droplet Epitaxy
Shichen Zhang, Li Liu, Kai Guo, Xingli Mu, Yuanfei Gao, Junqi Liu, Fengqi Liu, Quanyong Lu, and Zhiliang Yuan
Chin. Phys. Lett. **43**, 010402 (2026)

A series journal of Chinese Physical Society distributed by IOP Publishing

Chinese Physics Letters

Chin. Phys. Lett. **43** 120402 (2026)

LETTER

DOI: 10.1088/0256-307X/43/12/120402
CSTR: 32039.14.0256-307X.43.12.120402

Interference-Controlled Nonclassical Photon Emission via Cavity-Mediated Spin Exchange

Jing Tang[1,2] and Yuangang Deng[3,*]

[1]School of Physics and Optoelectronic Engineering, Guangdong University of Technology, Guangzhou 510006, China
[2]Guangdong Provincial Key Laboratory of Sensing Physics and System Integration Applications, Guangdong University of Technology, Guangzhou 510006, China
[3]Guangdong Provincial Key Laboratory of Quantum Metrology and Sensing & School of Physics and Astronomy, Sun Yat-Sen University, Zhuhai 519082, China

[*]Corresponding author. Email: dengyg3@mail.sysu.edu.cn

The generation of nonclassical light with strong photon antibunching and appreciable brightness remains an important goal in quantum technologies. Here, we demonstrate that cavity-mediated spin-exchange interactions provide a route to overcome this constraint by amplifying spectral anharmonicity. In a two-emitter cavity-QED system with a controllable relative phase ϕ, the resulting interference–interaction mechanism reshapes the dressed-state manifold and enables switching between distinct quantum emission regimes. For $\phi = 0$, constructive interference yields high-quality single-photon emission with near-perfect antibunching, suppressing $g_1^{(2)}(0)$ by more than three orders of magnitude while maintaining a substantial intracavity photon population. Conversely, for $\phi = \pi$, destructive interference suppresses direct single-photon excitation and selectively enhances two-photon excitation, producing signatures of correlated two-photon emission with appreciable intracavity photon populations and suppressed higher-order excitations. Our work establishes interference-engineered interactions as a mechanism for the controllable selection of single-photon and photon-pair emission, opening new opportunities for programmable nonclassical light sources and quantum photonic applications.

Introduction

Engineering light–matter interactions is central to quantum information and simulations [1−3]. Recent advances in ultracold quantum gases coupled to optical cavities provide powerful platforms to explore strongly correlated many-body physics under controllable light–matter coupling [4−6]. In particular, infinite-range cavity-mediated spin-exchange interactions (SEIs) have enabled the realization of diverse collective phenomena, including superradiant lasing [7], nonequilibrium quantum dynamics [8−11], and dark superradiance in polar molecules [12]. In parallel, optical tweezer arrays of neutral atoms and polar molecules provide a highly controllable setting that combines single-particle addressability with programmable long-range interactions [13−15], enabling controlled studies of collective radiation [16−19], symmetry-protected phases [20,21], quantum-enhanced sensing [22−24], and deterministic entanglement generation [25−28].

Meanwhile, nonclassical light ranging from antibunched single photons [29–33] to strongly correlated multiphoton states [34–36] constitutes a central resource for quantum networks [37,38], quantum communication [39,40], and quantum-enhanced metrology [41–44]. Despite significant progress, high-fidelity multiphoton emission typically relies on strong intrinsic optical nonlinearities, which remain challenging to achieve and control in experiments [45–47]. Harnessing collective long-range interactions to engineer effective optical nonlinearities and controllable photon statistics remains largely unexplored, offering a promising route toward controllable nonclassical photonic states [48,49].

In this Letter, we introduce a controllable scheme for nonclassical light generation by harnessing interaction-enhanced spectral anharmonicity in a two-emitter cavity-QED system. By adiabatically eliminating a far-detuned auxiliary cavity, a tunable cavity-mediated SEI is engineered between the two atoms. The interplay of SEI and phase-programmable interference establishes two distinct regimes of nonclassical photon emission. For $\phi = 0$, constructive interference cooperates with SEI-induced anharmonicity, enhancing strong photon blockade and reducing the second-order correlation $g_1^{(2)}(0)$ by more than three orders of magnitude while maintaining an appreciable intracavity photon population. In contrast, for $\phi = \pi$, destructive interference isolates a dark single-photon manifold, suppressing single-photon excitation while resonantly activating two-photon channels and inhibiting higher-order processes, even at moderate SEI strength. This mechanism enables bright, strongly correlated two-photon bundle emission under experimentally accessible conditions [7−10].

Remarkably, we uncover a direct correspondence between atomic spin correlations and photon statistics, characterized by a pronounced alternation of spin–spin correlations: positive (negative) transverse and negative (positive) longitudinal correlations accompany single-photon (multiphoton) emission, providing a diagnostic signature for identifying nonclassical emission regimes. Unlike approaches based on Mollow physics [34], parametric down-conversion [50], multiphoton resonance [51], or parity-symmetry-protected mechanisms [52], our scheme combines phase-selective coupling to collective atomic excitations with a tunable cavity-mediated spin-exchange interaction. The coupling phase controls optical access to different collective states, while the spin-exchange interaction modifies the dressed-state spectrum and its anharmonicity. Their interplay enables the selection of single- and two-photon emission regimes within the same cavity-QED system. This phase- and SEI-controlled mechanism may be extended to larger emitter arrays to access higher-order multiphoton emission [53], offering a promising route toward controllable nonclassical light sources based on cavity-mediated atomic interactions [54–56].

Model and Hamiltonian

We consider two identical atoms trapped in a one-dimensional optical tweezer array along the y axis and coupled to two orthogonal optical cavities with wave vector k, as illustrated in Fig. 1(a). Each atom is modeled as a two-level system consisting of a ground state $|g\rangle$ and a long-lived excited state $|e\rangle$, which may correspond to dipole-forbidden ${}^1S_0 \leftrightarrow {}^3P_1$ transition of alkaline-earth atoms, featuring a narrow

Received 23 August 2026; accepted 28 October 2026; published 17 November 2026
© 2026 Chinese Physical Society and IOP Publishing Ltd. All rights, including for text and data mining, AI training, and similar technologies, are reserved.

Check for updates

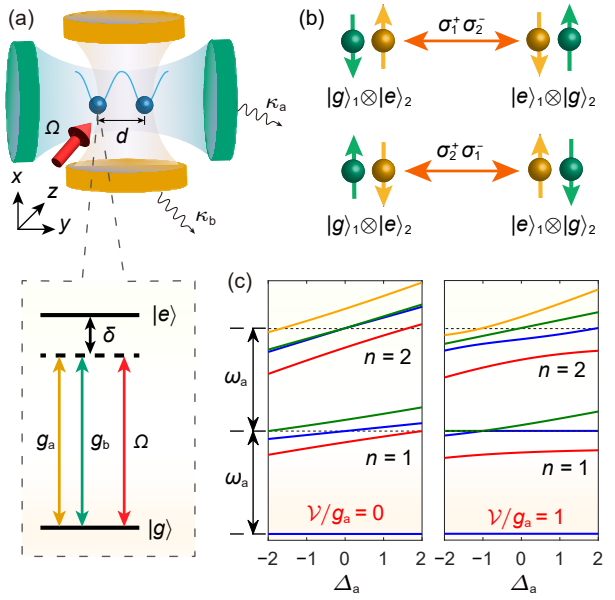

Fig. 1. Cavity-mediated SEIs engineer anharmonic energy structures in a two-emitter cavity-QED system. (a) Schematic of the two-emitter cavity-QED system. (b) Illustration of the cavity-mediated SEI. (c) Δ_a-dependent anharmonic energy spectrum highlighting interaction-induced level shifts.

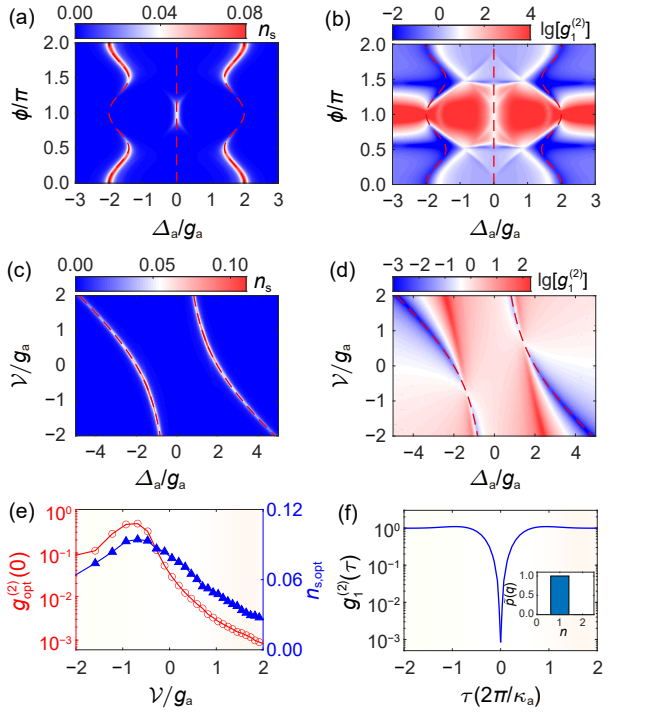

Fig. 2. Phase- and interaction-controlled photon statistics in the cavity-coupled system. (a) and (b) Steady-state photon number n_s and second-order correlation $g_1^{(2)}(0)$ as functions of Δ_a and ϕ for $\mathcal{V}=0$ and $\delta/\Delta_a = 1/2$, showing pure interference effects. (c) and (d) n_s and $g_1^{(2)}(0)$ versus Δ_a and $\mathcal{V}$ for $\phi/\pi = 0$, revealing interaction-induced modification of photon statistics. The red-dashed lines in (a)–(d) represent the analytically derived single-photon resonance curves. (e) Optimal $g_{opt}^{(2)}(0)$ (red line) and corresponding $n_{s,opt}$ (blue line) as functions of $\mathcal{V}$ along $\Delta_a = -\mathcal{V} - \sqrt{\mathcal{V}^2+4g_a^2}$. (f) Time-dependent correlation $g_1^{(2)}(\tau)$ at $\mathcal{V}/g_a = 2$. The inset shows the photon-number-weighted distribution $\tilde{p}(q)$ in the single-photon emission regime.

spontaneous decay $\gamma = (2\pi)7.5$ kHz [57]. The optical transition $|g\rangle \leftrightarrow |e\rangle$ couples to two cavity modes with single-atom cavity coupling g_a (g_b) and cavity decay κ_a (κ_b), respectively. Cavity mode A is chosen to be resonant with atomic transition, while cavity B operates in the far-detuned dispersive regime, with light-cavity detunings Δ_a and Δ_b. In addition, the atoms are driven by a transverse pump field with Rabi frequency Ω.

In the far-dispersive limit $|g_b/\Delta_b| \ll 1$, the auxiliary cavity B can be adiabatically eliminated, yielding an effective spin-exchange interaction between the two atoms. The derivation and validity conditions of the effective Hamiltonian are provided in the Supplementary Materials (SM). The resulting effective Hamiltonian for atoms coupled to cavity A is given by

$$\hat{\mathcal{H}}_1 = \Delta_a\hat{a}^\dagger\hat{a} + \frac{1}{2}\sum_{j=1}^{2}(\delta\hat{\sigma}_j^z + \Omega\hat{\sigma}_j^x) + \mathcal{V}\sum_{j\neq k}\hat{\sigma}_j^+\hat{\sigma}_k^- + g_a\hat{a}^\dagger(\hat{\sigma}_1^- + \cos\phi\,\hat{\sigma}_2^-) + \text{H.c.}, \tag{1}$$

where $\hat{a}$ denotes the cavity-field annihilation operator, $\hat{\sigma}_j^{x,y,z}$ are Pauli operators for atom j, and $\phi = kd$ is the relative coupling phase determined by the interatomic separation d along cavity A, with the first atom positioned at a standing-wave antinode. The atom-cavity coupling varies as $g_a\cos(ky_j)$, allowing ϕ to be controlled by adjusting the relative atomic positions. In the orthogonal-cavity geometry, the atoms can be displaced along cavity A while maintaining their coordinates along the axis of auxiliary cavity B. Thus, the coupling phase can be varied without changing the axial coupling phases of cavity B. Switching between $\phi = 0$ and $\phi = \pi$ requires a relative displacement of $\lambda/2$, corresponding to approximately 345 nm for the 689-nm transition of ^{88}Sr. Such positioning can, in principle, be achieved using individually controlled optical tweezers [58]. Provided that the displacement is small compared with the transverse mode waist of cavity B, its coupling strength and the resulting SEI remain approximately unchanged. Both operating points correspond to extrema of the standing-wave coupling, where small phase deviations affect the coupling amplitude only to second order. The phase-dependent photon statistics in Fig. 2 further illustrate the behavior away from these ideal configurations.

The cavity-mediated SEI is $\mathcal{V} = -g_b^2\Delta_b/[\Delta_b^2 + (\kappa_b/2)^2]$ and $\delta = \delta_c + \mathcal{V}$, with δ_c being the bare atom-pump detuning. The cavity-mediated SEI is effectively long-range within the single-mode description, as atoms coupled to the same auxiliary cavity mode can interact without conventional distance-dependent decay. Its applicability is limited by the cavity-mode profile and the validity of the single-mode, Markovian, and adiabatic approximations, rather than extending to arbitrarily large physical separations. The SEI shifts the collective atomic excitation energies [Fig. 1(b)] and modifies the dressed-state spectrum.

The dressed states are eigenstates of the Hamiltonian within each excitation manifold. In the single-excitation manifold, the bright polariton states arise from the hybridization of the cavity photon state and the collective atomic state coupled to the cavity field. For ($\phi = 0$) and ($\phi = \pi$), the orthogonal atomic dark state is decoupled from the cavity mode. Their eigenenergies define the corresponding dressed-state branches. Figure 1(c) illustrates the Δ_a-dependent dressed-state energy spectrum of the two-emitter cavity-QED system. The spectral anharmonicity characterizes the unequal spacing between successive excitation manifolds and can be quantified by $\mathcal{A}_{\mu\nu} = |E_{2,\nu} - 2E_{1,\mu}|$, where $E_{n,\mu}$ denotes the dressed-state energy in the n-excitation manifold, with the ground-state energy set to zero. This quantity measures the mismatch between successive transition frequencies along a specified dressed-state pathway. The dependence of the dressed-state spectrum on the SEI can be seen explicitly from the splitting of the single-excitation bright states at $\phi = 0$, $\Delta E_1 = \sqrt{(\delta+\mathcal{V}-\Delta_a)^2 + 8g_a^2}$. The SEI therefore modifies the bright-state splitting and the relative positions of the excitation manifolds. Three (four) dressed-state branches appear in the single- (two-) excitation manifold. For $\mathcal{V} = 0$, two degenerate dark states appear at $\Delta_a = 0$ in the $n \geq 2$ excitation manifolds, giving rise to three single-photon resonance points. In contrast, for $\mathcal{V}/g_a = 1$ and $\phi = \pi$, the degeneracy of dark states is lifted, leaving a single dark state protected by destructive quantum interference. The SEI modifies the spectral anharmonicity, while phase-controlled interference determines the optical accessibility of the dressed states.

Their interplay enables selective excitation of different excitation manifolds and control of nonclassical photon emission.

To characterize quantum correlations of the emitted nonclassical light, we describe the nonequilibrium dynamics of the system by a Lindblad master equation that incorporates all relevant dissipation channels,

$$\frac{\mathrm{d}\rho}{\mathrm{d}t} = -\mathrm{i}[\hat{\mathcal{H}}_1, \rho] + \kappa_\mathrm{a}\mathcal{D}[\hat{a}]\rho + \gamma\sum_{j=1}^{2}\mathcal{D}[\hat{\sigma}_j^-]\rho + \Gamma_\mathrm{e}\mathcal{D}[\hat{S}^-]\rho, \tag{2}$$

where ρ is the density matrix of the two-emitter cavity-QED system, $\mathcal{D}[\hat{o}]\rho = \hat{o}\rho\hat{o}^\dagger - (\hat{o}^\dagger\hat{o}\rho + \rho\hat{o}^\dagger\hat{o})/2$ denotes the standard Lindblad dissipator, and $\hat{S}^- = \hat{\sigma}_1^- + \hat{\sigma}_2^-$. Adiabatic elimination of the auxiliary cavity also induces collective decay at a rate $\Gamma_\mathrm{e} = \kappa_\mathrm{b}g_\mathrm{b}^2/[\Delta_\mathrm{b}^2 + (\kappa_\mathrm{b}/2)^2]$ [7]. In the far-dispersive regime $|\Delta_\mathrm{b}| \gg \kappa_\mathrm{b}$, we have $\Gamma_\mathrm{e}/|\mathcal{V}| = \kappa_\mathrm{b}/|\Delta_\mathrm{b}| \ll 1$. We therefore neglect this weak collective decay in the main numerical calculations.

The generalized kth-order correlation function is then defined as [34,59]

$$g_n^{(k)}(\tau_1,\ldots,\tau_k) = \frac{\left\langle\prod_{i=1}^{k}[\hat{a}^\dagger(\tau_i)]^n\prod_{i=k}^{1}[\hat{a}(\tau_i)]^n\right\rangle}{\prod_{i=1}^{k}\langle[\hat{a}^\dagger(\tau_i)]^n[\hat{a}(\tau_i)]^n\rangle}. \tag{3}$$

Here, $0 \le \tau_1 \le \cdots \le \tau_k$ denote chronologically ordered detection times, with the first detection time set to zero by stationarity. The correlation functions are normally and time ordered, with creation (annihilation) operators arranged in chronological (reverse chronological) order. For $n = 1$, $g_1^{(2)}(0) < 1$ indicates sub-Poissonian photon statistics, while $g_1^{(2)}(0) < g_1^{(2)}(\tau)$ characterizes photon antibunching for $\tau > 0$. For two-photon emission, $g_1^{(2)}(0) > 1$ together with $g_1^{(3)}(0) < 1$ indicates enhanced two-photon correlations and suppressed higher-order excitations [31]. Furthermore, $g_1^{(2)}(0) > g_1^{(2)}(\tau)$ and $g_2^{(2)}(0) < g_2^{(2)}(\tau)$ are characteristic signatures of photon bunching within two-photon bundles and antibunching between successive bundles, respectively [34,51]. These time-dependent criteria are examined for positive delays $\tau > 0$. For a Markovian cavity with vacuum input, the normally ordered intracavity correlations directly characterize the unfiltered output-field correlations through the standard input-output relation. These correlation criteria characterize photon-counting statistics but do not, by themselves, determine the purity of a selected propagating two-photon state. A characterization of specific temporal or spectral output modes requires an additional mode-resolved analysis [60–62].

In the absence of SEI ($\mathcal{V} = 0$), the n-excitation manifold ($n \ge 2$) supports two degenerate dark states at $\Delta_\mathrm{a} = \delta = 0$ for $\phi = 0$ $(-)$ and $\phi = \pi$ $(+)$, given by

$$\begin{aligned}|\psi_{n,A_\mp}\rangle &= \frac{1}{\sqrt{2}}(|n-1,g,e\rangle \mp |n-1,e,g\rangle),\\ |\psi_{n,S_\mp}\rangle &= \sqrt{\frac{n-1}{2n-1}}|n,g,g\rangle \mp \sqrt{\frac{n}{2n-1}}|n-2,e,e\rangle,\end{aligned} \tag{4}$$

with $\delta/\Delta_\mathrm{a} = 1/2$. These dark states originate from distinct physical mechanisms. The collective atomic state $|\psi_{n,A_\mp}\rangle$ becomes decoupled from the cavity field when $g_\mp = 0$, owing to destructive interference between the two atomic coupling pathways. The second class of dark states $|\psi_{n,S_\mp}\rangle$ arises from interference between excitation pathways involving different photon numbers, which cancels their coupling to the intermediate single-atom excitation states under the corresponding resonance condition. Consequently, direct single-photon excitation can be suppressed while resonant two-photon excitation remains accessible, enabling selective two-photon bundle emission through effective two-photon transitions $|2,g,g\rangle \leftrightarrow |0,e,e\rangle$ [63]. This mechanism is distinct from interference schemes in which photon emission is completely suppressed [18].

Numerical Results

The quantum statistics of nonclassical light are obtained by solving the master Eq. (2) in the limit of negligible auxiliary-cavity-induced collective decay. In the numerical simulation, we choose experimentally realistic parameters: $g_\mathrm{a} = 2\pi\times 120$ kHz and $\kappa_\mathrm{a} = 2\pi\times 15$ kHz [57,64,65], $g_\mathrm{b} = 2\pi\times 5$ MHz and $\kappa_\mathrm{b} = 2\pi\times 0.5$ MHz [16–18], and a weak transverse drive $\Omega/\kappa_\mathrm{a} = 0.2$. By tuning the auxiliary cavity in the far-dispersive regime $|\Delta_\mathrm{b}| > 2\pi\times 100$ MHz, the cavity-mediated SEI can be continuously controlled over the range $\mathcal{V}/g_\mathrm{a} \in [-2,2]$. The associated auxiliary-cavity-induced collective decay rate is $\Gamma_\mathrm{e} = \kappa_\mathrm{b}g_\mathrm{b}^2/[\Delta_\mathrm{b}^2 + (\kappa_\mathrm{b}/2)^2] < 2\pi\times 1.25$ kHz [7]. These parameters are compatible with those reported in cavity-QED experiments.

Single-Photon Emission

Figures 2(a) and 2(b) show the steady-state photon number n_s and zero-delay second-order correlation function $g_1^{(2)}(0)$ in the Δ_a–ϕ plane for $\mathcal{V} = 0$. Pronounced photon emission occurs along three resonance branches: two sidebands at $\Delta_\mathrm{a}/g_\mathrm{a} = \pm\sqrt{2(1+\cos^2\phi)}$, associated with the upper and lower bright polariton states in the single-excitation manifold, and a central branch at $\Delta_\mathrm{a} = 0$. For two bright polariton branches, n_s decreases monotonically with increasing ϕ and is strongly suppressed at $\phi = \pi$. At $\phi = 0$, the emitted field exhibits strong photon antibunching, with $g_1^{(2)}(0) \simeq 2.7\times 10^{-2}$, reflecting constructive to destructive quantum interference in single-photon excitation channel.

In contrast, n_s along the central branch increases monotonically with ϕ. At $\phi = \pi$, destructive interference selectively blocks single-photon excitation, allowing correlated multiphoton processes to dominate. Both dark states $|\psi_{n,A_+}\rangle$ and $|\psi_{n,S_+}\rangle$ in Eq. (4) are symmetric under particle exchange, leaving higher-order multiphoton excitations accessible. Remarkably, photon statistics exhibit a sharp transition to strong bunching with $g_1^{(2)}(0) \simeq 10$ [Fig. 2(b)], signaling multiphoton emission enabled by single-photon dark state formation. This phase-controlled antibunching–bunching transition is fundamentally distinct from conventional photon blockade [29–33], as it originates from tunable quantum interference rather than purely from spectral anharmonicity.

Introducing SEI strongly reshapes the anharmonic energy spectrum and substantially enhances the optical nonlinearity [Fig. 1(c)]. Figures 2(c) and 2(d) show n_s and $g_1^{(2)}(0)$ as functions of $\mathcal{V}$ and Δ_a. Because the antisymmetric state $|\psi_{n,A_-}\rangle$ is strongly decoupled for the central branch, the cavity response is dominated by the two bright states. Accordingly, $g_1^{(2)}(0)$ exhibits a pronounced dependence on both magnitude and sign of $\mathcal{V}$. The resulting red-blue-detuning asymmetry is consistent with the analytically predicted single-photon resonance positions $\Delta_\mathrm{a} = -\mathcal{V} \pm \sqrt{\mathcal{V}^2 + 4g_\mathrm{a}^2}$.

To quantify the optimal single-photon performance, we extract $g_\mathrm{opt}^{(2)}(0) = \min[g_1^{(2)}(\Delta_\mathrm{a})]$ and the corresponding $n_\mathrm{s,opt}$ at the same detuning as a function of $\mathcal{V}$ [Fig. 2(e)]. Remarkably, $g_\mathrm{opt}^{(2)}(0)$ remains well below unity across the entire interaction range, indicating robust photon antibunching at sideband resonances. Compared with the noninteracting case ($\mathcal{V} = 0$), the minimum second-order correlation is reduced by approximately two orders of magnitude, reaching $g_\mathrm{opt}^{(2)}(0) = 8\times 10^{-4}$ at $\mathcal{V}/g_\mathrm{a} = 2$, although the corresponding photon population $n_\mathrm{s,opt}$ decreases.

The time-dependent second-order correlation function $g_1^{(2)}(\tau)$ in Fig. 2(f) further confirms photon antibunching, with $g_1^{(2)}(0) < g_1^{(2)}(\tau)$ at short delays and a subsequent relaxation toward unity. Consistently, the steady-state photon-number distribution $\tilde{p}(q) = qp(q)/n_\mathrm{s}$ with $p(q) = \mathrm{Tr}\langle q|\rho|q\rangle$ is strongly concentrated at single-photon state, yielding $\tilde{p}(1) \approx 0.99998$ and negligible contributions from higher photon number. These results confirm that the observed strong antibunching originates from SEI-enhanced spectral anharmonicity.

In contrast to the conventional Jaynes–Cummings model, the photon statistics can be further controlled through the atomic detuning δ in the presence of SEI. The interaction shifts the energy of the bright collective atomic state, thereby modifying the dressed-state resonances. In particular, the single-photon resonance condition $\Delta_\mathrm{a} = 2g_\mathrm{a}^2/(\delta+\mathcal{V})$ shows that the resonance shifts toward larger $|\Delta_\mathrm{a}|$ as $|\delta+\mathcal{V}|$ approaches zero. High-quality single-photon emission therefore emerges from SEI-amplified optical nonlinearity. To elucidate

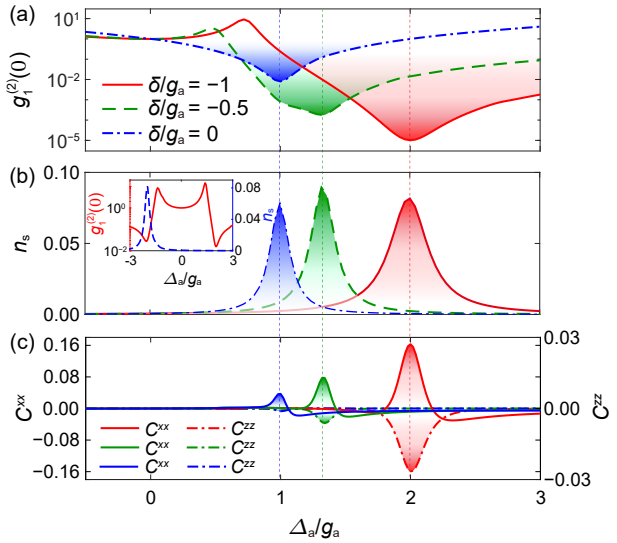

Fig. 3. Competition between detuning and interaction in shaping photon statistics and spin correlations. (a)–(c) $g_1^{(2)}(0)$, n_s, and spin correlations $C^{\mu\mu}$ as functions of Δ_a for different δ at fixed $\mathcal{V}/g_a = 2$. The inset in (b) shows the corresponding $g_1^{(2)}(0)$ and n_s for $\mathcal{V} = 0$ and $\delta/g_a = -1$, highlighting the absence of interaction-induced enhancement.

this behavior, we plot $g_1^{(2)}(0)$ and n_s as a function of Δ_a for different values of δ at fixed $\mathcal{V}/g_a = 2$ [Figs. 3(a) and 3(b)]. As Δ_a increases, photon antibunching is rapidly enhanced, reflecting the SEI-induced shift of the single-excitation resonance, arising from the modified effective atomic detuning $\delta + \mathcal{V}$. Remarkably, photon number remains nearly unchanged even deep in the strong photon-blockade regime with $g_1^{(2)}(0) = 1 \times 10^{-5}$. By tuning the atomic detuning δ at fixed $\mathcal{V}/g_a = 2$, the second-order correlation is reduced by more than three orders of magnitude relative to the noninteracting case ($\mathcal{V} = 0$) shown in the inset of Fig. 3(b), while maintaining a comparable intracavity photon population ($n_s \simeq 0.08$).

The coexistence of strong antibunching and an appreciable intracavity photon population demonstrates the potential for nonclassical single-photon emission through SEI-enhanced optical nonlinearity. This behavior stands in sharp contrast to conventional photon blockade schemes [29–33], where enhanced antibunching typically occurs at the cost of strongly reduced photon number. Notably, such enhancement is entirely absent for $\mathcal{V} = 0$, underscoring the essential role of long-range SEI in amplifying spectral anharmonicity.

Further physical insight is provided by examining connected spin correlations $C^{\mu\mu} = \langle \hat{\sigma}_1^{\mu} \hat{\sigma}_2^{\mu} \rangle - \langle \hat{\sigma}_1^{\mu} \rangle \langle \hat{\sigma}_2^{\mu} \rangle$ with $\mu = x, z$ [66]. Figure 3(c) shows the transverse correlation C^{xx} (solid line) and longitudinal correlation C^{zz} (dashed-dotted line) as a function of Δ_a for different δ. As δ decreases, C^{xx} becomes strongly positive while C^{zz} becomes strongly negative, indicating enhanced transverse spin coherence accompanied by anti-ferromagnetic correlations along the z axis. These correlations directly shape photon statistics: positive C^{xx} enhances collective emission within single-excitation manifold, boosting photon number, whereas negative C^{zz} suppresses double excitation, enforcing strong antibunching. The resulting synergy between collective emission and reinforced photon blockade enables the simultaneous realization of high brightness and pronounced single-photon antibunching. Remarkably, these results identify the detuning δ as a powerful control knob for engineering nonclassical light in the presence of long-range SEI. Strong antibunching can be achieved while maintaining an almost constant photon number, offering a route toward strongly antibunched single-photon sources.

Two-Photon Bundle Emission

We now turn to the regime $\phi = \pi$, where direct single-photon excitation is strongly suppressed by destructive quantum interference. Crucially, this interference-engineered spectrum offers a microscopic switching mechanism between single-photon ($\phi = 0$) and two-photon bundle ($\phi = \pi$) emission. Figures 4(a)–4(c) display phase-space maps of n_s, $g_1^{(2)}(0)$, and $g_1^{(3)}(0)$ as functions of $\mathcal{V}$ and Δ_a at $\delta/\mathcal{V} = -1$. Two distinct resonance branches appear at $\Delta_a = -g_a^2/\mathcal{V}$ and $\Delta_a = 2\mathcal{V}$. Near these resonances, $g_1^{(2)}(0) \gg 1$ and $g_1^{(3)}(0) \ll 1$, indicating strong photon bunching accompanied by three-photon blockade.

To characterize the two-photon emission regime, we examine $g_1^{(2)}(0)$, $g_1^{(3)}(0)$, and n_s along the two resonance branches, as shown in Figs. 4(d) and 4(e). Along the branch $\Delta_a = -g_a^2/\mathcal{V}$, both correlations decrease as $\mathcal{V}$ decreases. Notably, photon bunching with $g_1^{(2)}(0) > 1$ and strong three-photon blockade with $g_1^{(3)}(0) \sim 10^{-4}$ persist even for a weak SEI ($\mathcal{V}/g_a < 0.48$). These results demonstrate that pronounced two-photon correlations and suppression of higher-order excitations can coexist with a finite cavity population at moderate SEI strengths. Along the branch $\Delta_a = 2\mathcal{V}$, $g_1^{(2)}(0)$ increases slightly with $\mathcal{V}$, while $g_1^{(3)}(0)$ decreases nonmonotonically, reaching a minimum of approximately 10^{-2} with $n_s \simeq 0.04$.

These features originate from phase-controlled quantum interference at $\phi/\pi = 1$, which suppresses direct single-photon excitation while leaving the two-excitation manifold resonantly accessible. The SEI provides an additional control parameter for tuning the positions and strengths of the two-photon resonances. Figure 4(f) displays Δ_a-dependence of photon statistics for a weak interaction $\mathcal{V}/g_a = 0.4$, demonstrating pronounced two-photon bunching and strong suppression of three-photon correlations on both sidebands, together with appreciable cavity populations. By contrast, two-photon emission at central branch vanishes when $\mathcal{V} = 0$. Achieving comparable performance without SEI would require an unrealistically small dissipation ratio $\gamma/\kappa_a \ll 1$. Notably, even moderate SEI strongly suppresses $g_1^{(3)}(0)$, highlighting the role of the interaction in controlling higher-order photon correlations.

Further insight is obtained by examining the connected spin correlation $C^{\mu\mu}$ as a function of Δ_a [Fig. 4(g)]. Different from single-photon regime, two-photon resonance exhibits a distinct correlation signature: transverse component C^{xx} is strongly suppressed, while longitudinal component C^{zz} becomes significantly less negative. This behavior reflects the inhibition of single-excitation processes and the enhanced participation of double excitations. Consistently, the time-dependent correlation functions $g_1^{(2)}(\tau)$ and $g_2^{(2)}(\tau)$ [Fig. 4(h)] exhibit $g_1^{(2)}(0) > g_1^{(2)}(\tau)$ and $g_2^{(2)}(\tau) > g_2^{(2)}(0)$ over the relevant short-time interval. These opposite temporal correlations indicate photon bunching within pairs and antibunching between successive pair events, providing evidence for two-photon bundle emission. The photon-number-weighted distribution $\tilde{p}(q)$ shows appreciable contributions from the single- and two-photon occupations, with $\tilde{p}(1) \approx 0.71$ and $\tilde{p}(2) \approx 0.29$, while higher-order contributions are strongly suppressed, $\sum_{q>2} \tilde{p}(q) \approx 7 \times 10^{-6}$. These results provide correlation-based evidence for two-photon bundle emission with suppressed higher-order excitations, but do not directly quantify the purity or relative occurrence rate of emitted photon pairs. A quantitative characterization of photon-pair emission purity would require additional output photon-counting statistics or quantum-trajectory analysis [34].

Discussion

We have introduced a versatile scheme in which a programmable atomic phase, combined with cavity-mediated SEI, enables controlled switching between single-photon and photon-pair bundle emission. The central resource is the interplay of phase-controlled quantum interference and SEI-induced spectral anharmonicity, which selectively addresses distinct excitation manifolds and produces strongly antibunched single-photon emission or bright correlated two-photon emission. In the latter regime, destructive interference suppresses direct single-photon excitation while retaining resonant access to the two-excitation manifold. These regimes exhibit distinct transverse and longitudinal spin-correlation signatures, establishing atomic spin correlations as a direct and versatile diagnostic of nonclassical photon emission.

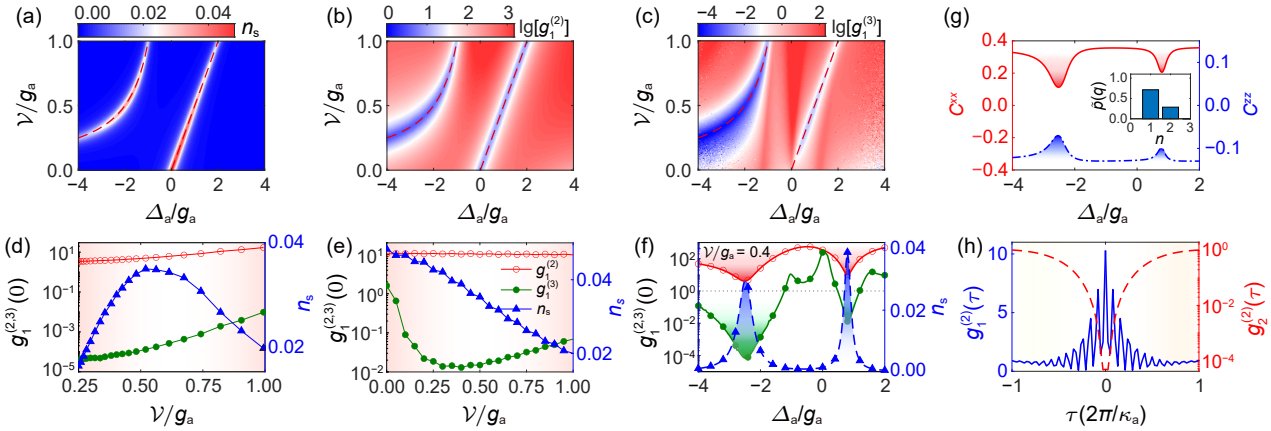

Fig. 4. Interaction-driven multiphoton correlations and spin-order signatures. (a)–(c) Photon number n_s, second-order $g_1^{(2)}(0)$, and third-order $g_1^{(3)}(0)$ correlations in the $\mathcal{V}$–Δ_a plane for $\delta/\mathcal{V} = -1$ and $\phi/\pi = 1$, revealing multiphoton regimes. (d) and (e) $g_1^{(2,3)}(0)$ and n_s along the trajectories (d) $\Delta_a = -g_a^2/\mathcal{V}$ and (e) $\Delta_a = 2\mathcal{V}$, respectively. (f) Δ_a-dependent $g_1^{(2,3)}(0)$ and n_s at fixed $\mathcal{V}/g_a = 0.4$. (g) Corresponding spin correlations $C^{\mu\mu}$. (h) Time-dependent $g_1^{(2)}(\tau)$ (blue) and $g_2^{(2)}(\tau)$ (red) for $\Delta_a = 2\mathcal{V} = 0.8g_a$.

More broadly, our results demonstrate that collective interactions can overcome the intrinsic limitations of few-emitter nonlinearities. In particular, maintaining high brightness while dramatically enhancing photon antibunching alleviates the conventional blockade trade-off and provides a route toward bright nonclassical light sources. The established correspondence between spin correlations and photon statistics further elevates the two-emitter cavity-QED system to a dual-function platform: a programmable source of engineered nonclassical light and a controllable platform for investigating collective light–matter dynamics. The phase-controlled interference mechanism may be extended to two-dimensional arrays and cascaded cavity architectures [67–69], providing opportunities to explore higher-order multiphoton emission and correlations in larger systems. Our work thus establishes interference-engineered interactions as a promising route toward bright nonclassical photon sources, opening new opportunities in quantum metrology, networked quantum information processing, and the exploration of collective quantum dynamics [25–28].

Acknowledgments

This work was supported by the National Natural Science Foundation of China (Grant Nos. 12674338, 12374365, 12274473, and 12135018), Guangdong Provincial Quantum Science Strategic Initiative (Grant Nos. GDZX2604004 and GDZX2505001), and Quantum Science and Technology-National Science and Technology Major Project (Grant No. 2025ZD0300400).

References

[1] Bloch I, Dalibard J, and Zwerger W 2008 *Rev. Mod. Phys.* **80** 885
[2] Saffman M, Walker T G, and Mølmer K 2010 *Rev. Mod. Phys.* **82** 2313
[3] Defenu N, Donner T, Macrì T, Pagano G, Ruffo S, and Trombettoni A 2023 *Rev. Mod. Phys.* **95** 035002
[4] Ritsch H, Domokos P, Brennecke F, and Esslinger T 2013 *Rev. Mod. Phys.* **85** 553
[5] Forn-Díaz P, Lamata L, Rico E, Kono J, and Solano E 2019 *Rev. Mod. Phys.* **91** 025005
[6] Mivehvar F, Piazza F, Donner T, and Ritsch H 2021 *Adv. Phys.* **70** 1
[7] Norcia M A, Lewis-Swan R J, Cline J R K, Zhu B, Rey A M, and Thompson J K 2018 *Science* **361** 259
[8] Muniz J A, Barberena D, Lewis-Swan R J, Young D J, Cline J R K, Rey A M, and Thompson J K 2020 *Nature* **580** 602
[9] Luo C, Zhang H, Koh V P W, Wilson J D, Chu A, Holland M J, Rey A M, and Thompson J K 2024 *Science* **384** 551
[10] Niu Z, Schäfer V M, Zhang H, Wagner C, Taylor N R, Young D J, Song E Y, Chu A, Rey A M, and Thompson J K 2025 *Phys. Rev. Lett.* **134** 113403
[11] You J, Yi S, and Deng Y 2025 *Photon. Res.* **13** 987
[12] Wang Y, Yi S, and Deng Y 2025 arXiv:2504.18125 [cond-mat.quant-gas]
[13] Ebadi S, Wang T T, Levine H, Keesling A, Semeghini G, Omran A, Bluvstein D, Samajdar R, Pichler H, Ho W W, Choi S, Sachdev S, Greiner M, Vuletić V, and Lukin M D 2021 *Nature* **595** 227
[14] Barredo D, De Léséleuc S, Lienhard V, Lahaye T, and Browaeys A 2016 *Science* **354** 1021
[15] Anderegg L, Cheuk L W, Bao Y, Burchesky S, Ketterle W, Ni K K, and Doyle J M 2019 *Science* **365** 1156
[16] Léonard J, Morales A, Zupancic P, Esslinger T, and Donner T 2017 *Nature* **543** 87
[17] Yan Z, Ho J, Lu Y H, Masson S J, Asenjo-Garcia A, and Stamper-Kurn D M 2023 *Phys. Rev. Lett.* **131** 253603
[18] Liu Y, Wang Z, Yang P, Wang Q, Fan Q, Guan S, Li G, Zhang P, and Zhang T 2023 *Phys. Rev. Lett.* **130** 173601
[19] Han Y, Li H, and Yi W 2024 *Phys. Rev. Lett.* **133** 243401
[20] De Léséleuc S, Lienhard V, Scholl P, Barredo D, Weber S, Lang N, Büchler H P, Lahaye T, and Browaeys A 2019 *Science* **365** 775
[21] Yue Z, Mao Y F, Liang X, Hua Z X, Ge P, Chao Y X, Li K, Jia C, Tey M K, Xu Y, and You L 2026 *Nat. Phys.* **22** 844
[22] Marciniak C D, Feldker T, Pogorelov I, Kaubruegger R, Vasilyev D V, van Bijnen R, Schindler P, Zoller P, Blatt R, and Monz T 2022 *Nature* **603** 604
[23] Kaubruegger R, Silvi P, Kokail C, van Bijnen R, Rey A M, Ye J, Kaufman A M, and Zoller P 2019 *Phys. Rev. Lett.* **123** 260505
[24] Schäffner D, Schreiber T, Lenz F, Schlosser M, and Birkl G 2024 *PRX Quantum* **5** 010311
[25] Wilk T, Gaëtan A, Evellin C, Wolters J, Miroshnychenko Y, Grangier P, and Browaeys A 2010 *Phys. Rev. Lett.* **104** 010502
[26] Holland C M, Lu Y, and Cheuk L W 2023 *Science* **382** 1143
[27] Bao Y, Yu S S, Anderegg L, Chae E, Ketterle W, Ni K K, and Doyle J M 2023 *Science* **382** 1138
[28] Schine N, Young A W, Eckner W J, Martin M J, and Kaufman A M 2022 *Nat. Phys.* **18** 1067
[29] Birnbaum K M, Boca A, Miller R, Boozer A D, Northup T E, and Kimble H J 2005 *Nature* **436** 87
[30] Dayan B, Parkins A S, Aoki T, Ostby E P, Vahala K J, and Kimble H J 2008 *Science* **319** 1062
[31] Hamsen C, Tolazzi K N, Wilk T, and Rempe G 2017 *Phys. Rev. Lett.* **118** 133604
[32] Zhou Y H, Liu T, Su Q P, Zhang X Y, Wu Q C, Chen D X, Shi Z C, Shen H Z, and Yang C P 2025 *Phys. Rev. Lett.* **134** 183601
[33] Lu Z G, Wu Y, and Lü X Y 2025 *Phys. Rev. Lett.* **134** 013602
[34] Sánchez Muñoz C, del Valle E, González Tudela A, Müller K, Lichtmannecker S, Kaniber M, Tejedor C, Finley J J, and Laussy F P 2014 *Nat. Photonics* **8** 550
[35] Liu C, Huang J F, and Tian L 2023 *Sci. China Phys. Mech. Astron.* **66** 220311
[36] Bin Q, Jing H, Wu Y, Nori F, and Lü X Y 2024 *Phys. Rev. Lett.* **133** 043601

[37] Ritter S, Nölleke C, Hahn C, Reiserer A, Neuzner A, Uphoff M, Mücke M, Figueroa E, Bochmann J, and Rempe G 2012 *Nature* **484** 195
[38] Redjem W, Zhiyenbayev Y, Qarony W, Ivanov V, Papapanos C, Liu W, Jhuria K, Al Balushi Z Y, Dhuey S, Schwartzberg A, Tan L Z, Schenkel T, and Kanté B 2023 *Nat. Commun.* **14** 3321
[39] Duan L M, Lukin M D, Cirac J I, and Zoller P 2001 *Nature* **414** 413
[40] Kimble H J 2008 *Nature* **453** 1023
[41] Niemietz D, Farrera P, Langenfeld S, and Rempe G 2021 *Nature* **591** 570
[42] Giovannetti V, Lloyd S, and Maccone L 2011 *Nat. Photonics* **5** 222
[43] Kozlov M G, Safronova M S, Crespo López-Urrutia J R, and Schmidt P O 2018 *Rev. Mod. Phys.* **90** 045005
[44] Pezzè L, Smerzi A, Oberthaler M K, Schmied R, and Treutlein P 2018 *Rev. Mod. Phys.* **90** 035005
[45] Paredes R, Bruun G, and Camacho-Guardian A 2024 *Phys. Rev. A* **110** 030101
[46] Chakram S, He K, Dixit A V, Oriani A E, Naik R K, Leung N, Kwon H, Ma W L, Jiang L, and Schuster D I 2022 *Nat. Phys.* **18** 879
[47] Carl L, Rosa-Medina R, Huber S D, Esslinger T, Dogra N, and Dubcek T 2023 *Phys. Rev. Res.* **5** L032003
[48] Defenu N, Lerose A, and Pappalardi S 2024 *Phys. Rep.* **1074** 1
[49] Young D J, Chu A, Song E Y, Barberena D, Wellnitz D, Niu Z, Schäfer V M, Lewis-Swan R J, Rey A M, and Thompson J K 2024 *Nature* **625** 679
[50] Chang Y, González-Tudela A, Sánchez Muñoz C, Navarrete-Benlloch C, and Shi T 2016 *Phys. Rev. Lett.* **117** 203602
[51] Deng Y, Shi T, and Yi S 2021 *Photon. Res.* **9** 1289
[52] Bin Q, Wu Y, and Lü X Y 2021 *Phys. Rev. Lett.* **127** 073602
[53] Tang J and Deng Y 2026 *Phys. Rev. A* **114** 053702
[54] Neuzner A, Körber M, Morin O, Ritter S, and Rempe G 2016 *Nat. Photon.* **10** 303
[55] Wang H, Ralph T C, Renema J J, Lu C Y, and Pan J W 2025 *Nat. Mater.* **24** 1883
[56] Tang J and Deng Y 2024 *Phys. Rev. Res.* **6** 033247
[57] Winchester M N, Norcia M A, Cline J R K, and Thompson J K 2017 *Phys. Rev. Lett.* **118** 263601
[58] Norcia M A, Young A W, and Kaufman A M 2018 *Phys. Rev. X* **8** 041054
[59] del Valle E, Gonzalez-Tudela A, Laussy F P, Tejedor C, and Hartmann M J 2012 *Phys. Rev. Lett.* **109** 183601
[60] Yang J, Strandberg I, Vivas-Viaña A, Gaikwad A, Castillo-Moreno C, Kockum A F, Ullah M A, Muñoz C S, Eriksson A M, and Gasparinetti S 2025 *npj Quantum Inf.* **11** 69
[61] Vivas-Viaña A, and Sánchez Muñoz C 2026 *PRX Quantum* **7** 010346
[62] López Carreño J C, Bermúdez Feijoo S, and Stobińska M 2024 *npj Nanophoton.* **1** 3
[63] Zhao G, Chen Y, Zhang J, Tang J, and Deng Y 2025 arXiv:2512.01250 [quant-ph]
[64] Peters M L, Wang G, Spierings D C, Drucker N, Hu B, Chen M W, Chen Y T, and Vuletić V 2025 *Phys. Rev. Lett.* **135** 093402
[65] Kongkhambut P, Skulte J, Mathey L, Cosme J G, Hemmerich A, and Keßler H 2022 *Science* **377** 670
[66] Puel T O and Macrì T 2024 *Phys. Rev. Lett.* **133** 106901
[67] Ferreira V S, Kim G, Butler A, Pichler H, and Painter O 2024 *Nat. Phys.* **20** 865
[68] Bluvstein D, Evered S J, Geim A A, Li S H, Zhou H, Manovitz T, Ebadi S, Cain M, Kalinowski M, Hangleiter D, Bonilla Ataides J P, Maskara N, Cong I, Gao X, Sales Rodriguez P, Karolyshyn T, Semeghini G, Gullans M J, Greiner M, Vuletić V, and Lukin M D 2024 *Nature* **626** 58
[69] O'Sullivan J, Reuer K, Grigorev A, Dai X, Hernández-Antón A, Muñoz-Arias M H, Hellings C, Flasby A, Colao Zanuz D, Besse J C, and Eichler C 2025 *Nat. Commun.* **16** 5505